Biophysical Properties of Camelid V_{HH} Domains Compared to Those of Human V_H3 Domains†

Stefan Ewert,‡ Christian Cambillau,§ Katja Conrath,|| and Andreas Plückthun*,‡

Biochemisches Institut, Universität Zürich, Winterthurerstrasse 190, CH-8057 Zürich, Switzerland, Architecture et Fonction des Macromolecules Biologiques, CNRS, 31 Chemin Joseph Aiguier, F-13402 Marseille Cedex 20, France, and Vrije Universiteit Brussel, Vlaams Interuniversitair instituut voor biotechnologie, Department ultrastructure, Paardenstraat 65, B-1640 St. Genesius Rode, Belgium

Received June 15, 2001; Revised Manuscript Received December 13, 2001

ABSTRACT: *Camelidae* possess an unusual form of antibodies lacking the light chains. The variable domain of these heavy chain antibodies (V_{HH}) is not paired, while the V_H domain of all other antibodies forms a heterodimer with the variable domain of the light chain (V_L), held together by a hydrophobic interface. Here, we analyzed the biophysical properties of four camelid V_{HH} fragments (H14, AMD9, RN05, and CA05) and two human consensus V_H3 domains with different CDR3 loops to gain insight into factors determining stability and aggregation of immunoglobulin domains. We show by denaturant-induced unfolding equilibria that the free energies of unfolding of V_{HH} fragments are characterized by ΔG_{N-U} values between 21.1 and 35.0 kJ/mol and thus lie in the upper range of values for V_H fragments from murine and human antibodies. Nevertheless, the V_{HH} fragments studied here did not reach the high values between 39.7 and 52.7 kJ/mol of the human consensus V_H3 domains with which they share the highest degree of sequence similarity. Temperature-induced unfolding of the V_{HH} fragments that were studied proved to be reversible, and the binding affinity after cooling was fully retained. The melting temperatures were determined to be between 60.1 and 66.7 °C. In contrast, the studied V_H3 domains aggregated during temperature-induced denaturation at 63−65 °C. In summary, the camelid V_{HH} fragments are characterized by a favorable but not unusually high stability. Their hallmark is the ability to reversibly melt without aggregation, probably mediated by the surface mutations characterizing the V_{HH} domains, which allow them to regain binding activity after heat renaturation.

Up to 75% of immunoglobulins found in the sera of *Camelidae* lack the light chain while still being functional (*1*). These "heavy chain antibodies" are homodimers, with each chain consisting of an unpaired variable domain (V_{HH})[1] immediately followed by a hinge region, C_H2 and C_H3 domain. X-ray structures of camelid V_{HH} domains showed a typical immunoglobulin fold with its β-sandwich scaffold (*2*−*4*). Nevertheless, V_{HH} domains possess some remarkable properties, which clearly distinguish them from the variable domain (V_H) of a conventional antibody. Mutations of hydrophobic amino acids are found at the former interface, which contacts the V_L domain in conventional antibodies. These mutations [Val44Phe (or Tyr), Gly51Glu (or Gln), Leu52Arg (or Cys), and Trp54Gly (or Ser, Leu, or Phe)] [numbering according to the new consensus nomenclature of Honegger and Plückthun (*5*)] are highly conserved within the camel antibodies and are a key feature distinguishing them from a conventional V_H domain (*6*). Three hypervariable regions can be clearly distinguished in the V_{HH} sequences. CDR1 and CDR2 loops adopt new structures that fall outside the canonical structures described for human or mouse V_H loops (*3*). Furthermore, CDR1 of V_{HH} fragments may begin closer to the N-terminus in comparison to human or mouse CDRs (*7*). The CDR3 loop of V_{HH} fragments is on average longer (17 residues) than the human (12 residues) or mouse (9 residues) CDR3 loop (*8*, *9*). To stabilize the long CDR3, the V_{HH} domains often contain a second intradomain disulfide bond, which connects CDR3 with the end of CDR1 or with a core residue between CDR1 and CDR2 (*8*).

V_{HH} fragments have been considered to have great potential in various industrial applications. V_{HH} domains represent the smallest antigen-binding unit with a molecular size of ~15 kDa in comparison to scFv fragments (30 kDa), Fab fragments (60 kDa), and whole antibodies (150 kDa). They can be expressed in bacterial and yeast expression systems (*10*−*12*). Long CDR3 can generate new antigen binding modes, such as the one seen in the complex between the V_{HH} fragment Lys3 with lysozyme, where the extended CDR3 penetrates into the active side of the enzyme (*13*).

† This work was supported by EC Project BIO4-98-0048.

* To whom correspondence should be addressed. Telephone: (+41-1) 635 5570. Fax: (+41-1) 635 5712. E-mail: plueckthun@biocfebs.unizh.ch.

‡ Universität Zürich.

§ CNRS.

|| Universiteit Brussel.

[1] Abbreviations: CDR, complementary determining region; C_H1, constant domain 1 of the heavy chain of a normal antibody; GdnHCl, guanidine hydrochloride; IMAC, immobilized metal ion affinity chromatography; scFv, single-chain antibody fragment consisting of the variable domains of the heavy and light chains connected by a peptide linker; V_H, variable domain of the heavy chain of a human antibody; V_{HH}, variable domain of a camelid heavy chain antibody; V_L, variable domain of the light chain of a human antibody.

10.1021/bi011239a CCC: $22.00
Published on Web 02/19/2002

Therefore, a new class of inhibitory proteins based on V_{HH} domains could be envisaged. The most remarkable property of V_{HH} fragments is, however, their behavior at elevated temperatures. It has been shown that after exposure for 2 h to a temperature of >80 °C the antigen binding properties of some llama V_{HH} fragments are not reduced (*12*). Moreover, two llama V_{HH} fragments elicited against a hydrophobic azo dye still exhibited activity in a binding assay at 90 °C (*12*). These thermal properties make conceivable applications which were previously thought to be inaccessible.

What are the reasons for these favorable thermal properties? We were interested in distinguishing whether these molecules are unusually thermally stable and do not melt or whether instead they exhibit reversible melting behavior. Furthermore, we compared the V_{HH} molecules among themselves and with human V_H3 domains, their closest relative in conventional antibodies. We therefore analyzed the biophysical properties of four camelid V_{HH} fragments with known X-ray structures. We included in this study the llama V_{HH} fragment H14 elicited against the α-chain of human chorionic gonadotropin hormone (hCG) (*4*) and three camel V_{HH} fragments [RN05 which binds to RNase A (*2*), CA05 elicited against carbonic anhydrase (*3*), and AMD9 which binds to amylase (*14*)]. We determined the free energy of unfolding (ΔG_{N-U}) of all fragments from denaturant-induced unfolding and refolding equilibria, analyzed the temperature-induced denaturation properties, and determined melting temperatures (T_m). In addition, we measured these data for two human germline consensus V_H3 domains with different CDR3 loops. We then compared the X-ray structures of H14, AMD9, RN05, and CA05 (*2*−*4*) with structures determined for V_H3 domains to provide an explanation for the observed thermodynamic properties.

As from initial studies extraordinary thermodynamic properties and expression behavior of camelid antibody domains had been proposed, we investigated their thermodynamic properties in more detail. If there had been unusual structural properties, they could possibly be engineered into human V_H domains as well. While our analysis indeed points to favorable properties, none of the four fragments that were investigated had unusually high expression yields in *Escherichia coli* or reached the equilibrium stabilities of the human V_H3 consensus domains, which can in principle be even further stabilized by interaction with stable V_L domains in an scFv or Fab fragment. We show that the most unique property of camelid V_{HH} domains is their ability to melt *reversibly*, which not only facilitates their study but also opens the door for applications where transient heating may occur.

RESULTS

Expression and Protein Purification. The V_{HH} fragments H14, AMD9, RN05, and CA05 (*2*, *12*, *14*) and the human germline consensus V_H3 domains (*15*) with two different CDR3 loops were expressed in soluble form in the periplasm of *E. coli* fused to a C-terminal hexahistidine tag. The long CDR3 (used in V_H3-L) had been obtained from a metabolic selection (J. Burmester et al., unpublished results) and was found to lead to soluble domains, while the short loop (V_H3-S) is derived from the well-expressed antibody 4D5 (*15*, *16*). The proteins were purified from the soluble fraction of the cell extracts by IMAC followed by preparative gel filtration chromatography in the case of the V_{HH} fragments, or IMAC followed by cation exchange chromatography in the case of the V_H3 fragments. A yield of 1.2 mg/L of bacterial culture could be obtained for CA05, while the yield was ∼4 mg/L for AMD9 and RN05. The highest yield was found for H14 with 7.4 mg/L of bacterial culture, which is the least stable domain (see below). However, the higher yield could be due to the use of a different expression vector (*17*) and/or the coexpression of Skp, which had been found to enhance the functional expression yield of scFv fragments in the periplasm of *E. coli* (*18*). The human V_H3 domain with the long CDR3 loop (termed V_H3-L, 17 residues) gave a yield of 1.8 mg of soluble protein and the one with the short CDR3 loop (termed V_H3-S, 9 residues) a yield of 0.2 mg of soluble protein from 1 L of bacterial culture.

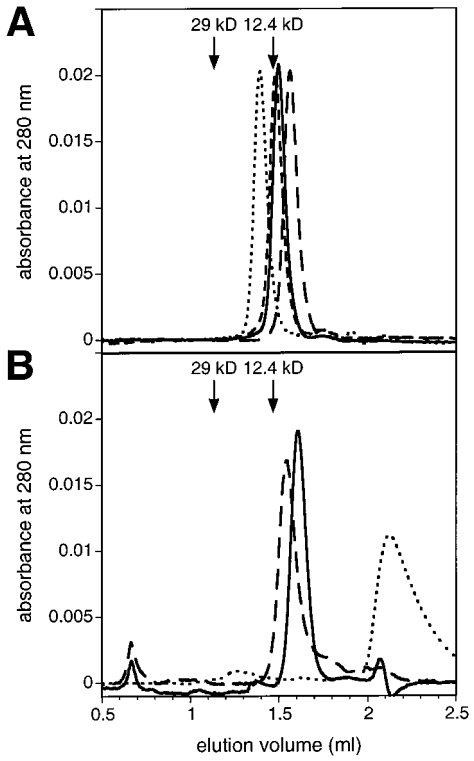

FIGURE 1: Analytical gel filtration of (A) camel V_{HH} fragments (each 2 μM) H14 (···), AMD9 (− − −), RN05 (—), and CA05 (- - -) and (B) human V_H3 fragments V_H3-S (—) and V_H3-L (− − −) in 50 mM sodium phosphate (pH 7.0) and 100 mM NaCl and V_H3-S (···) in 1 M GdnHCl, 50 mM sodium phosphate (pH 7.0), and 100 mM NaCl applied on a Superdex-75 column. Arrows indicate elution volumes of the molecular mass standards carbonic anhydrase (29 kDa) and cytochrome *c* (12.4 kDa).

Analytical gel filtration experiments with protein concentrations of 2 μM showed that AMD9, RN05, CA05, and V_H3-L elute in 50 mM sodium phosphate (pH 7.0) and 100 mM NaCl with an apparent molecular mass of ∼14 kDa, which corresponds to the size of a monomer (Figure 1A,B). Under these conditions, V_H3-S elutes in a broad peak at an apparent molecular mass much smaller than 12.4 kDa, but in the presence of 1 M GdnHCl, it elutes at the expected volume (Figure 1B), indicating that under native buffer conditions this fragment interacts with the column material. V_H3-S also has a tendency to aggregate upon prolonged standing at 4 °C, while the camelid fragments and V_H3-L stay in solution. This behavior of V_H3-S may be due to the

stickiness of the hydrophobic interface, which is normally covered by V_L in human antibodies. In V_H3-L, this interface may be partially covered by long CDR3 in the absence of the V_L domain.

Equilibrium Transition Experiments. The thermodynamic stability of the V_{HH} and V_H3 fragments was determined by GdnHCl equilibrium denaturation experiments. Unfolding and refolding of the V_{HH} domains as a function of denaturant concentration were monitored by the change in the fluorescence intensity at the wavelength with the biggest difference between folded and unfolded spectra (Figure 2A with AMD9 as an example for V_{HH} domains). While the fluorescence intensity of H14, AMD9, and RN05 decreases during the unfolding transition, the intensity of CA05 increases (data not shown). This different behavior of CA05 might be explained by the additional disulfide bridge between Cys128 and Cys40, which possibly quenches the fluorescence intensity of Trp116 in the native but not in the denatured state. Unfolding of V_H3-L and V_H3-S was followed by the shift in the fluorescence emission maximum at increasing denaturant concentrations, because the change in fluorescence intensity between the native and denatured state was only small (Figure 2B with VH3-L as an example for V_H3 domains). The equilibrium denaturation of all domains is cooperative and reversible (Figure 2), which is an indication of two-state behavior. Figure 2C shows an overlay of the equilibrium denaturation and renaturation curves of H14, AMD9, RN05, CA05, V_H3-L, and V_H3-S, normalized to show the fraction of unfolded protein. V_H3-L and V_H3-S exhibit the highest change in free energy upon unfolding (ΔG_{N-U}) with values of 52.7 and 39.7 kJ/mol, respectively. CA05 displays the highest ΔG_{N-U} of the camelid V_{HH} domains with a value of 35.0 kJ/mol, followed by RN05 with a ΔG_{N-U} of 31.7 kJ/mol (Table 1). H14 and AMD9 are less stable and have ΔG_{N-U} values of 21.9 and 21.1 kJ/mol, respectively. The range of m values is between 14.1 and 17.4 kJ mol^{-1} M^{-1} and is thus in the range expected for proteins of this size (14−15 kDa) (*19*). This indicates that all V_{HH} and V_H3 fragments that were examined have the cooperativity expected for a two-state transition.

Temperature-Induced Denaturation. To follow the reversible temperature-induced unfolding, the V_{HH} fragments were heated and cooled at a constant rate of 0.5 °C/min, and the fluorescence intensity at 344 nm was recorded as a function of temperature. Figure 3A shows the relative fluorescence intensity during temperature-induced de- and renaturation for AMD9 as an example for the V_{HH} fragments. After the fragments had been cooled, more than 80% of the fluorescence signal was recovered for all the V_{HH} fragments that were studied. The incomplete recovery of the fluorescence signal may be due to some irreversible denaturation but also to some chemical changes at high temperatures such as oxidation of sulfur species or deamidation for Asn and Gln at elevated temperatures (*20*), which would alter the fluorescence intensity of the native protein. For all V_{HH} fragments, a single transition of denaturation was observed, which is consistent with two-state behavior. Again, the fluorescence intensity at the unfolding transition decreases in the cases of H14, AMD9, and RN05 and increases in the case of CA05.

An overlay of the temperature-induced denaturation curves of the V_{HH} fragments that were studied is shown in Figure 3B. CA05 shows the highest T_m (66.7 °C), followed by RN05 and AMD9 with values of 64.2 and 64.1 °C, respectively. H14 displays the lowest T_m (60.1 °C, Table 1). The thermodynamic parameters were estimated by a fit with the combined eqs 1 and 2. However, there is a large error in this method, as it involves seven parameters. Therefore, we are not reporting ΔH_m and ΔC_p values. Nevertheless, ΔC_p values can be estimated from the dependence on the change in the accessible surface area upon unfolding (*19*). Using this fixed ΔC_p in the fit, ΔH_m values were obtained ranging

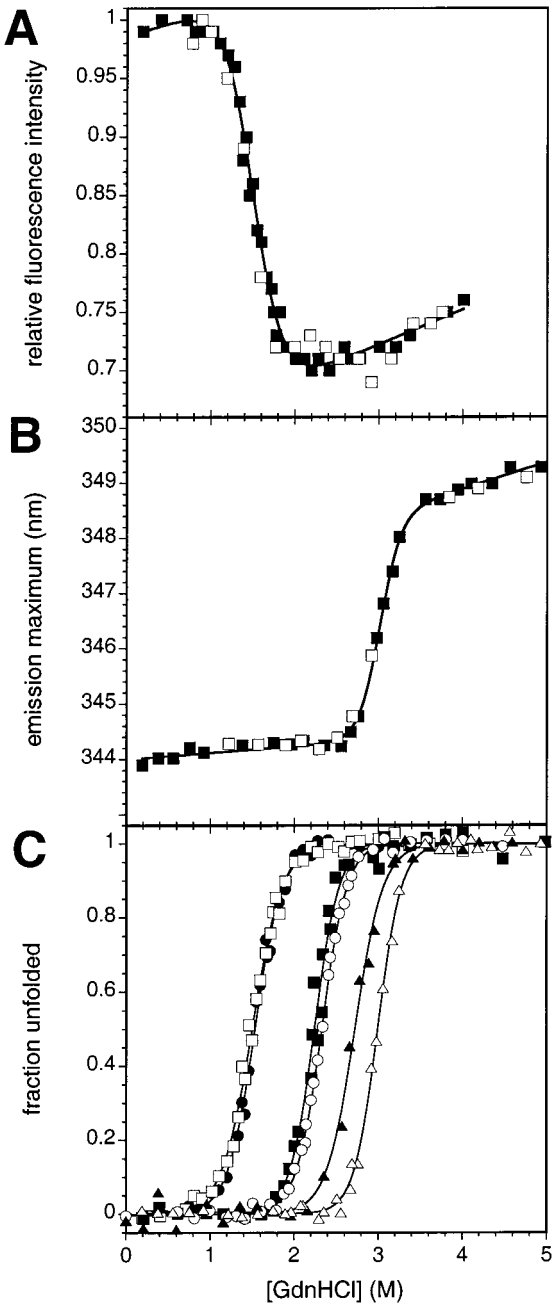

FIGURE 2: GdnHCl denaturation of (A) AMD9 and (B) V_H3-L. Unfolding (■) and refolding (□) transitions were measured by following the change in fluorescence intensity at 345 nm (AMD9, panel A) or the shift in emission spectra maxima (V_H3-L, panel B) as a function of denaturant concentration at an excitation wavelength of 280 nm. In panel A, the highest fluorescence intensity of the curve was set to 1 to obtain the relative fluorescence intensity. (C) Overlay of GdnHCl denaturation and renaturation curves of H14 (●), AMD9 (○), RN05 (■), CA05 (□), V_H3-S (▲), and V_H3-L (△). Curves in panel C are normalized to the fraction of unfolded protein.

Table 1: Summary of Biophysical Characterization of V_{HH} Fragments

					denaturant-induced denaturation			temperature denaturation	
	name	species	no. of disulfide bonds	CDR3 length	midpoint [GdnHCl] (M)	ΔG_{N-U} (kJ/mol)	m (kJ M^{-1} mol^{-1})	T_m (°C)	maintained activity (%)[b]
V_{HH}	H14	llama	1	7	1.54	21.9	14.4	60.1	73 ± 7
	AMD9	camel	1	13	1.51	21.1	14.1	64.1	92 ± 8
	RN05	camel	1	11	2.21	31.7	14.4	64.2	97 ± 5
	CA05	camel	2	18	2.35	35.0	15.0	66.7	98 ± 7
V_H3	L	human	1	17	3.00	52.7	17.4	65.2[a]	nd[c]
	S	human	1	10	3.20	39.7	14.6	63.4[a]	nd[c]

[a] Onset of aggregation. [b] After heating to 80 °C and cooling to room temperature. [c] Not determined.

from 400 to 550 kJ/mol and ΔG(298 K) values were estimated, which are ~30% higher than those determined from the denaturant-induced equilibrium transition experiments, but this is still within the combined error range of both methods (data not shown).

The binding activity maintained after temperature treatment of the V_{HH} fragments at a concentration of 0.5 μM was tested using ELISAs (Table 1). Under the conditions that were examined, H14 retained 73% of its binding activity in comparison to the untreated sample, while AMD9, RN05, and CA05 retained 92−98% of their activity.

In contrast to the reversible behavior of the V_{HH} fragments during temperature-induced denaturation, V_H3-L and -S precipitated at higher temperatures. Therefore, the protein samples were heated at a constant rate of 0.5 °C/min from 20 to 80 °C, and light scattering was recorded as a function of temperature. Temperature-induced protein aggregation results in an increase in scattered light intensity at 500 nm at a particular temperature followed by a steep increase (Figure 3C). The onset of thermal aggregation is at 65.2 and 63.4 °C for V_H3-L and V_H3-S, respectively (see Experimental Procedures). For the V_{HH} fragments, no increase in scattered light intensity was observed.

Analysis of the Sequence Alignment and X-ray Structure. A sequence alignment (Figure 4) between camel V_{HH} and human V_H3 fragments shows a high level of homology. The hydrophobic core residues with side chain solvent accessibility of <10% (marked with × in Figure 4) are especially highly conserved. Only at position 31 (Phe in the human sequence and Tyr, Gly, or Val in the camelid sequence) and position 44 (Val in the human sequence and Phe in the camelid sequence) are there group specific differences. The conformation of the core residues at the base of the domains is strongly dependent on the amino acid at positions 10 and 78 (*21*). These positions are the same in the V_{HH} and V_H3 fragments (Gly10 and Phe78), which indicates similar packing and thus contribution to the overall stability. In contrast, the CDRs of the V_{HH} fragments, which also affect the core in the upper part, display larger differences in length and amino acid composition in comparison to human V_H3 domains (*7*).

Figure 5A shows a superposition of the structures of the V_{HH} fragments that have been studied [PDB entries 1HCV (*4*), 1BZQ (*2*), 1F2X (*3*), and 1KXQ (structure of AMD9, C. Cambillau et al., unpublished results)] in yellow and structures with human V_H3 domains [PDB entries 1AQK (*22*), 1DEE (*23*), 1IGM (*24*), and 2FB4 (*25*)] in blue. The CDR regions show large differences with respect to the V_H3 domains, leading to additional structures for CDR H1 and H2 loops different from the canonical structures of human and murine domains (*3*). These regions also have an influence on the packing of the upper part of the hydrophobic core. Panels C and D of Figure 5 show a detailed view of upper core residues 2, 25, 29, 31, 41, 89, and 108. Superpositions are shown of the V_{HH} structures of CA05 and AMD9, which are the most and least stable camel fragments, respectively, and the V_H3 domain of a human Fab fragment [PDB entry 1DEE (*23*)], which is most identical in sequence to the core residues of the consensus V_H3 domain.

All structures were checked for cavities in an effort to identify packing differences that could lead to fewer van der Waals interactions and, therefore, reduced thermodynamic stability. A van der Waals contact surface was generated for a water radius of 1.4 Å with the program MOLMOL (*26*). When cavities were found, the surrounding residues were checked for whether they would contribute hydrophobic surface area to the cavity, since a water molecule would be energetically unfavorable at such a position. These cavities found in the upper part of V_{HH} but not in the human V_H3 structures indicate poor packing and may be one of the contributing factors for the lower thermodynamic stability of the V_{HH} domains in comparison to the V_H3 consensus domain. In contrast, the architecture of the framework residues in the lower part of the V_{HH} fragments superimposes well with the V_H3 domains. The sequence alignment shows that lower core residues 19, 74, 78, 93, and 104 are identical in camel V_{HH} and human V_H3 domains, and indeed, they structurally superimpose (Figure 5B).

In addition, there are two minor differences between the camel and human domains. First, in the V_{HH} fragments, the "interface region to V_L" is altered because of exchanges of conserved residues [Val44 to Tyr or Phe, Gly51 and Leu52 to Glu51 and Arg52, respectively, and Trp54 to Gly (*8*)], giving this region a different chemical nature. Second, the outer loop of the V_{HH} domains shows a greater structural variability than that of V_H3 domains.

Conserved charged residues are distributed over the domains (marked with + in Figure 4). Some of them are involved in conserved buried salt bridges between the charged groups of Arg45 and Glu53, Arg45 and Asp100, and Arg77 and Asp100. This charge cluster has a similar conformation in the human consensus V_H3 domain {Figure 6A shows the KOL Fab fragment [PDB entry 2FB4 (*25*)], which has the highest level of sequence identity with respect to charged residues to the consensus V_H3 domain} and camel V_{HH} domains (Figure 6B with CA05 as an example for V_{HH} domains), indicating that both charge clusters should contribute similarly to the overall stability of the domains. However, there are two major differences between camelid V_{HH} and human V_H3 domains in terms of charged residues:

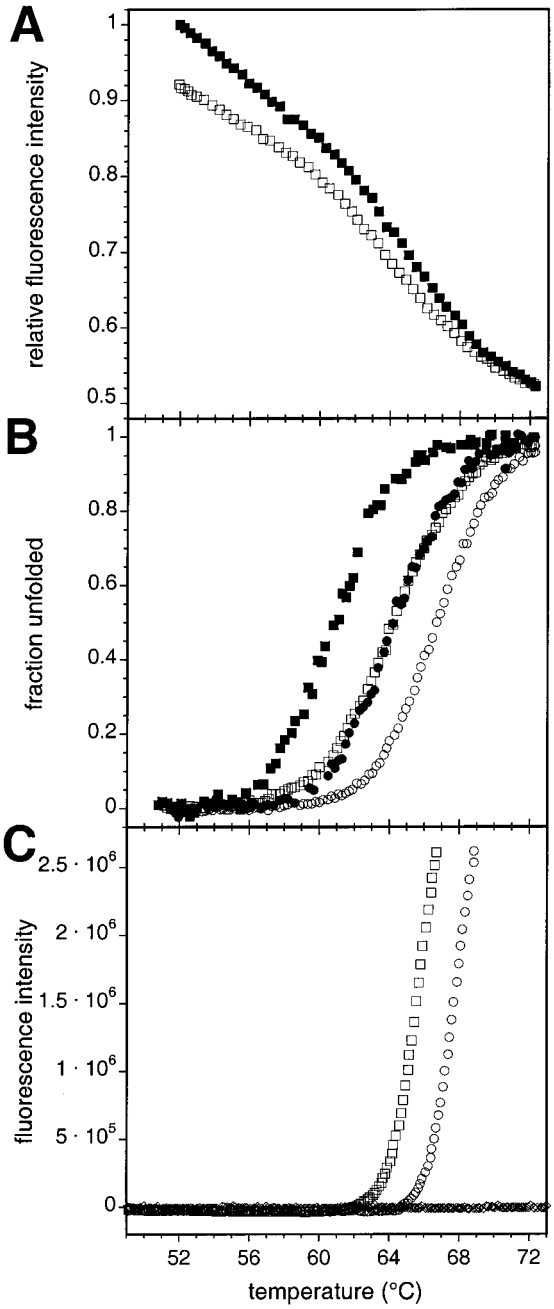

FIGURE 3: (A) Temperature-induced denaturation of AMD9. Unfolding (■) and refolding (□) transitions were measured by following the change in fluorescence intensity at 344 nm as a function of temperature. The fluorescence intensity at the lowest temperature of the unfolding curve was set to 1 to obtain the relative fluorescence intensity. (B) Overlay of temperature-induced unfolding transitions of H14 (■), AMD9 (□), RN05 (●), and CA05 (○). Curves are normalized to the fraction of unfolded protein. (C) Thermal aggregation of V_H3-S (□), V_H3-L (○), and AMD9 (×) as an example for V_{HH} domains monitored by light scattering at 500 nm as a function of the measured temperature in the cuvette.

(1) the already mentioned exchanges in the V_{HH} domains at the interface region at positions 51 and 52 from Gly and Leu to charged residues, which makes the molecule more soluble, and (2) the conserved salt bridge between Arg108 and Asp137 in V_H domains at the ends of the CDR3 loop (Figure 6A) that constrains the conformation of this CDR and may thus be crucial for antigen binding specificity (*27*, *28*). Its removal from a V_H domain decreases the melting temperature (*29*). Sequence analysis of V_{HH} domains shows that in camels the conserved Arg108 residue is exchanged to an uncharged residue unable to build a salt bridge to Asp137 (*8*) (Figure 6B). This change may be another factor contributing to the decreased stability of the V_{HH} domains that have been investigated in comparison to the consensus V_H3 domain.

Role of CDR3. A prominent feature of camel V_{HH} fragments is the length of the CDR3 loop. The length of 17 sequenced camel V_{HH} CDR3 regions ranges from 10 to 24 residues with an average of 17.5 residues (*8*). Human V_H domains have an average CDR3 length of 11.6 residues (*9*). Long CDR3 of camel V_{HH} domains can facilitate the penetration of this CDR into active site clefts and cavities in antigens, as seen in the cAb−Lys3−lysozyme complex (*13*). They may also cover the hydrophobic interface to V_L, as seen in the crystal structure of V_{HH} fragments RN05, CA05, R2, and Lys3 (*3*, *4*, *13*, *30*), thereby also rendering the domain more soluble. In some V_{HH} fragments, especially those with long CDR3 loops, there is an additional disulfide bridge connecting CDR3 with the end of CDR1 or with a core residue between CDR1 and CDR2. Interestingly, the presence of this additional disulfide bridge does not correlate with the thermodynamic stability, as seen in CA05 and RN05, which both differ only slightly in their ΔG_{N-U} values, but only CA05 has the additional disulfide bridge. Clearly, this comparison is not straightforward, since the 19-amino acid long CDR3 of CA05 may need further stabilization in the form of an additional disulfide bridge to be as stable as RN05 with an only 12-amino acid long CDR3. The human consensus V_H3 domains V_H3-L and -S differ only in their CDR3 loop, which varies in length and amino acid composition. This difference results in a 10-fold increase in the yield of soluble protein in the periplasm and a 10 kJ/mol increase in ΔG_{N-U}, for the domain with long CDR3 compared to the one with short CDR3. Probably, this long CDR3 covers part of the hydrophobic interface to V_L, thus taking on part of the stabilizing role of V_L as seen in V_{HH} structures, and therefore increases solubility, stability, and yield.

DISCUSSION

Our analysis of the biophysical properties of camel V_{HH} fragments has shown that these domains fold and unfold reversibly in denaturant- and temperature-induced denaturation experiments, and give results consistent with a two-state process. The V_{HH} fragments studied here show free energies of unfolding ΔG_{N-U} between 20.7 and 35.0 kJ/mol, values which lie in the upper range of those reported for V_H domains from human or murine antibodies (*31*−*33*). However, they are smaller than the high values of 52.7 and 39.7 kJ/mol found for the human consensus V_H3-L and V_H3-S domains, respectively, with which they share the highest degree of sequence similarity.

A comparison of the X-ray structures of these V_{HH} fragments to structures containing the V_H3 domain showed that both V_{HH} and V_H3 fragments have similar conformations of the charge cluster and the lower hydrophobic core residues, which should thus contribute to the stability in a similar way (Figures 5B and 6). The main difference found between the V_{HH} and V_H3 domains is the packing of the upper core, resulting from different CDR1 and CDR2 conformations, implying that this altered packing is involved

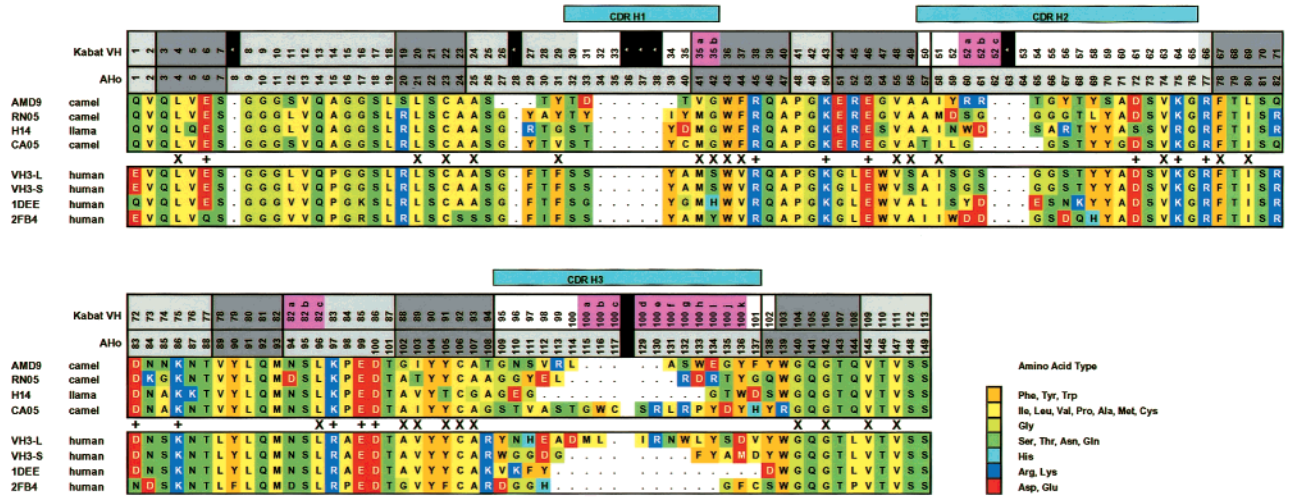

FIGURE 4: Sequence alignment of the V_{HH} fragments (*2*, *12*, *14*) that were studied, the human consensus V_H3-L and -S domains (*15*), and the VH3 domains of an anti-protein A Fab fragment [PDB entry 1DEE (*23*)] and KOL Fab fragment [PDB entry 2FB4 (*25*)] which are reference structures for discussing hydrophobic core packing (Figure 5) and stabilization through salt bridges (Figure 6). The amino acids are color-coded according to residue type: orange for aromatic residues (Tyr, Phe, and Trp), yellow for hydrophobic residues (Leu, Ile, Val, Met, Cys, Pro, and Ala), green for uncharged hydrophilic residues (Ser, Thr, Gln, Asn, and Gly), red for acidic residues (Asp and Glu), and blue for basic residues (Arg, Lys, and His). The symbol × indicates hydrophobic residues with side chain solvent accessibility of <10%, and the symbol + indicates conserved charged residues. Both numbering schemes according to Kabat et al. (*40*) and Honegger and Plückthun (*5*) are shown. The latter scheme is used throughout the text.

in the somewhat lower thermodynamic stability of the camelid V_{HH} fragments in comparison to the consensus V_H3 (Figure 5C,D).

Why might V_{HH} fragments sacrifice effective packing in the upper part? A human IgG antibody has six CDRs to bind to an antigen (three each from V_H and V_L). A camel heavy chain antibody has only three CDRs to bind to an antigen. To bind to a great variety of different antigens, the V_{HH} domain has to adapt, at least in the upper part, to a great variety of shapes at the possible expense of thermodynamic stability. Furthermore, the gain in stability upon binding to its antigen should be larger for a V_{HH} fragment, because its loose upper core is further stabilized in a complex with the antigen than the already more stable V_H3 upper core.

A striking difference between the camel V_{HH} and human consensus V_H3 domains was seen upon exposure to high temperatures. Unfolding occurs at about the same temperature. However, in contrast to the irreversible temperature-induced unfolding of the V_H3 domains, the V_{HH} domains that were studied did not aggregate during temperature denaturation, but could reversibly fold back to the native conformation upon cooling the sample. After temperature treatment, the binding activity of all studied V_{HH} fragments was fully retained as shown by ELISA experiments. This is consistent with the result of Perez et al. (*34*), who reported that the llama V_{HH} fragment H14 has a melting temperature of ~60 °C and folds reversibly back to its native conformation. Our results are further complemented by a study comparing properties of llama V_{HH} fragments (including H14) and mouse monoclonal antibodies at elevated temperatures (*12*). Incubation of these V_{HH} fragments for 2 h at temperatures greater than 80 °C had no significant effect on the binding capability of most of the llama V_{HH} fragments after cooling the sample, while mouse monoclonal antibodies were irreversibly inactivated. Our data strongly suggest that this is not because the llama V_{HH} domains do not denature, but rather because they reversibly refold upon cooling, which was also shown for the V_{HH} fragment H14. The conserved mutations in the interface region to V_L, a hallmark of V_{HH} domains (*8*), are making them more soluble (*35*) and are probably causing these differences. In contrast, mouse and human antibody V_H domains are built for a V_H/V_L association with a hydrophobic interface. If these molecules are thermally denatured, they aggregate and do not reversibly refold. However, in the V_H/V_L assembly, both domains can also further stabilize each other (*36*, *37*), and therefore, the stability of the V_H3 domain can be increased even further in an scFv or Fab format. Interestingly, the "camelized" V_H3 domain with the interface mutations (Gly51Glu, Leu52Arg, and Trp54Gly) but without the additional disulfide bridge connecting CDR3 with framework residue 40 shows a lower stability than the wild-type human V_H3 domain, demonstrating that the interface mutations increase solubility but decrease stability (*29*).

The alternative solution of solubilizing the V_H domain to form V_{HH} with longer loops gives camels an alternative option for binding to an antigen. As the antigen-binding interface is smaller, tight binding may be more challenging to achieve on a routine basis. On the other hand, all other antibody formats containing multiple interacting Ig domains, some of which are even more stable than V_{HH} domains, cannot be heated above the melting point, as denaturation leads to an irreversible aggregation, while camel V_{HH} domains refold upon cooling. It is this property which makes camel V_{HH} domains unique and interesting for biotechnological applications.

EXPERIMENTAL PROCEDURES

Expression Vectors. The expression vectors for the V_{HH} fragments AMD9, RN05, and CA05 (PH6AMD9His, PH6RN05His, and PH6CA05His, respectively) were kindly provided by S. Muyldermans (*2*, *14*). The V_{HH} fragment H14 was PCR amplified from the vector pUR4520-H14, which was kindly provided by L. G. Frenken (*12*), and expressed

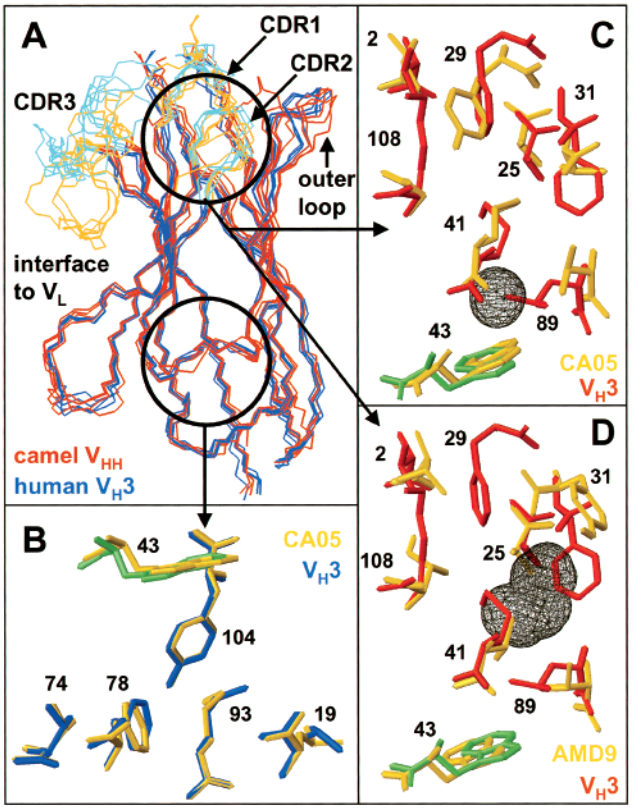

FIGURE 5: (A) Superposition of structures of V_{HH} fragments (PDB entries 1HCV, 1BZQ, 1F2X, and 1KXQ) in red (CDRs in orange) and structures with human V_H3 domains (PDB entries 1AQK, 1DEE, 1IGM, and 2FB4) in blue (CDRs in cyan). (B) Detailed view of the lower core. Superposition of CA05 (PDB entry 1F2X) in yellow and the V_H3 domain of an anti-protein A Fab fragment (PDB entry 1DEE) in blue. The conserved Trp43 is shown in green. (C and D) Detailed view of the upper core. Superposition of CA05 (PDB entry 1F2X) (C) and of AMD9 (PDB entry 1KXQ) (D) in yellow with the V_H3 domain of an anti-protein A Fab fragment (PDB entry 1DEE) in red. The conserved Trp43 is shown in green. The van der Waals contact surface was generated for a probe radius of 1.4 Å with the program MOLMOL (*26*). Cavities within the upper core of the V_{HH} fragments are shown in black. Images were generated using the program MOLMOL (*26*). Numbering scheme according to Honegger and Plückthun (*5*).

from a derivative of the vector pAK400 (*17*). The expression cassette of H14, which consists of a pelB signal sequence, the H14 gene, and a hexahistidine tag, was introduced between the *Xba*I and *Hin*dIII restriction sites, and the *skp* cassette (*18*) was introduced at the *Not*I restriction site.

The human germline consensus V_H3 domain was PCR amplified from a vector containing the V_H3-$(Gly_4Ser)_4$-$V_L\kappa3$ scFv master gene of the human combinatorial antibody library (HuCAL) from Morphosys (*15*), which carried CDR-H3 and CDR-L3 of the hu4D5-8 antibody (*16*). In addition, the CDR3 region between the *Bss*HII and *Sty*I restriction sites was then exchanged to encode a CDR-H3 (YNHEADMLIRNWLYSDV) found by metabolic selection (J. Burmester et al., unpublished results) to yield soluble V_H domains. The final expression plasmids were derivatives of the vector pAK400 (*17*), in which the expression cassette of the two human germline consensus V_H3 domains, which consists of a *phoA* signal sequence, the short FLAG tag (DYKD), the V_H3 domain, and a hexahistidine tag, had been introduced between the *Xba*I and *Hin*dIII restriction sites, and where the *skp* cassette (*18*) had been introduced at the *Not*I restriction site. The resulting human V_H3 domains are called V_H3-S and V_H3-L with S for "short CDR3" (10 residues) and L for "long CDR3" (17 residues).

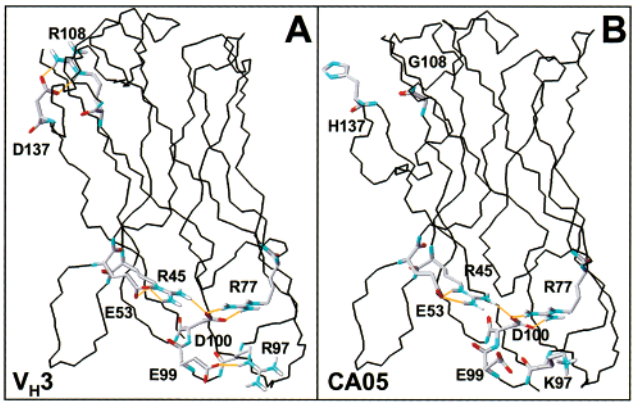

FIGURE 6: (A) V_H3 domain of the KOL Fab fragment (PDB entry 2FB4) and (B) CA05 (PDB entry 1F2X) as an example for V_{HH} fragments with residues colored by atom type which form putative salt bridges (orange). Images were generated using the program MOLMOL (*26*). Numbering scheme according to Honegger and Plückthun (*5*).

Protein Expression and Purification. Periplasmic expression was performed as described previously (*38*). Each His tag-containing protein was purified by immobilized metal ion affinity chromatography (IMAC) under native conditions on a nitrilotriacetic acid column (Qiagen), which had been charged with Ni^{2+}. In the case of the V_{HH} fragments, the eluate was loaded on a Superdex-75 column (Pharmacia) and preparative gel filtration chromatography was performed in 50 mM sodium phosphate (pH 7.0) and 100 mM NaCl. In the case of the V_H3 domains, the eluate was directly loaded onto a HQ anion exchange column in 50 mM Tris (pH 7.0) and 100 mM NaCl. Elution from the anion exchange column was achieved with a 0 to 800 mM NaCl gradient. Pooled fractions of all fragments were dialyzed against 50 mM sodium phosphate (pH 7.0) and 100 mM NaCl.

Analytical Gel Filtration Chromatography. Samples of purified V_{HH} and V_H3 domains were analyzed on a Superdex-75 column equilibrated with 50 mM sodium phosphate (pH 7.0) and 100 mM NaCl on a SMART system (Pharmacia). The domains were injected at a concentration of 2 μM in a volume of 50 μL, and the flow rate was 50 μL/min. Lysozyme (14 kDa) and carbonic anhydrase (29 kDa) were used as molecular standards.

Equilibrium Denaturation Experiments. Fluorescence spectra were recorded at 25 °C with a PTI Alpha Scan spectrofluorimeter (Photon Technologies, Inc.). Slit widths of 2 nm were used for excitation and emission. Protein/GdnHCl mixtures (2 mL) containing a final protein concentration of 0.5 μM and denaturant concentrations ranging from 0 to 5 M GdnHCl were prepared from freshly purified protein and a GdnHCl stock solution [8 M, in 50 mM sodium phosphate (pH 7.0) and 100 mM NaCl]. Each final concentration of GdnHCl was determined from its refractive index. After overnight incubation at 10 °C, the fluorescence emission spectra of the samples were recorded from 320 to 370 nm with an excitation wavelength of 280 nm. With increasing denaturant concentrations, the maxima of the recorded emission spectra shifted from ~342 to 348 nm.

Protein stabilities were calculated from the plot of fluorescence intensity at 335 (RN05), 337 (H14), and 345 nm (AMD9 and CA05) or the shift of the emission spectrum maximum (VH3-S and -L) versus GdnHCl concentration as described previously (*31*).

Temperature-Induced Denaturation (Reversible). The V_{HH} fragments were analyzed for their reversible thermal denaturation properties with a PTI Alpha Scan spectrofluorimeter. Excitation and emission wavelengths were 280 and 344 nm, respectively. The V_{HH} domains were measured in 50 mM sodium phosphate (pH 7.0) and 100 mM NaCl at a final protein concentration of 0.5 μM. After being filtered through 0.2 μm Millipore filters, the samples were heated in a 3 mL polymethyl methacrylate (PMMA) cuvette (Kartell) in a volume of 1.7 mL. The temperature was increased from 52 to 72 °C at a rate of 0.5 °C/min. The reversibility of temperature-induced denaturation was checked by cooling the sample to 52 °C with a temperature gradient of 0.5 °C/min. Intensities were measured every 15 s. Data analysis was performed assuming a two-state unfolding mechanism. The data were fitted to eqs 1 and 2 (*39*) using SigmaPlot (SPSS Inc.)

$$F_{obs}(T) = \{F_f + m_f T + (F_u + m_u T)\exp[-\Delta G(T)/RT]\}/\{1 + \exp[-\Delta G(T)/RT]\} \quad (1)$$

$$\Delta G(T) = \Delta H_m(1 - T/T_m) - \Delta C_p[T_m - T + T\ln(T/T_m)] \quad (2)$$

where $F_{obs}(T)$ is the observed fluorescence intensity at 344 nm at temperature T, F_f, F_u, m_f, and m_u represent intercepts and slopes of native and unfolded baselines, respectively, $\Delta G(T)$ is the free energy at temperature T, ΔH_m is the enthalpy change, T_m is the melting temperature, ΔC_p is the change in heat capacity, and R is the gas constant.

Temperature-Induced Denaturation (Irreversible). The V_H3 domains were analyzed for their irreversible thermal denaturation properties. The temperature of the onset of aggregation was determined by light scattering as described previously (*33*), using a PTI Alpha Scan spectrofluorimeter. Excitation and emission wavelengths were 500 nm. The V_H domains were measured in 50 mM sodium phosphate (pH 7.0) and 100 mM NaCl at a final protein concentration of 0.5 μM. After being filtered through 0.2 μm Millipore filters, the samples were heated in a 3 mL sealed quartz cuvette in a volume of 1.7 mL. A temperature gradient of 0.5 °C/min was applied, starting from 20 °C to the temperature of maximal intensity. Intensities were measured every 15 s. All measurements were performed in duplicate, and averaged values are given. After normalization, i.e., by setting the intensity of the pretransition region to zero for all V_H domains, the aggregation temperature was obtained from the intensity versus temperature plot by determining the intersection of the temperature axis and a linear fit of all points exceeding intensity values of 5×10^5.

Enzyme-Linked Immunosorbent Assay (ELISA). To test the residual binding activity after thermal denaturation, a temperature gradient from 52 to 72 °C and back to 52 °C was applied to purified V_{HH} fragments (0.5 °C/min) at a concentration of 0.5 μM in 50 mM sodium phosphate (pH 7.0), 100 mM NaCl, and 0.05% Tween 20. Human chorionic gonadotropin hormone (Sigma), porcine α-amylase (EC 3.2.1.1, type IA; Sigma), bovine pancreatic RNase A (EC 3.1.27.5; Sigma), and bovine erythrocyte carbonic anhydrase (EC 4.2.1.1; Sigma) at a concentration of 5 μg/mL in 50 mM sodium phosphate and 100 mM NaCl (pH 7.0) were applied overnight at 4 °C to coat Maxisorb 96-well plates (Nunc). Plates were blocked in 2.0% sucrose, 0.1% bovine serum albumin (EC 232.936.2; Sigma), and 0.9% NaCl for 2 h at room temperature. After incubation with either the untreated or heat-treated and subsequently renatured V_{HH} fragments, bound fragments were detected using the tetra-His antibody (Qiagen) followed by an anti-mouse antibody conjugated with alkaline phosphatase (Sigma). The percentage of binding activity maintained after temperature denaturation was calculated using triplicates at four different concentrations (10^{-1}, 10^{-2}, 10^{-3}, and 10^{-4} μM) of temperature-treated and untreated V_{HH} fragments.

ACKNOWLEDGMENT

We thank Drs. Serge Muyldermans, Lode Wyns (both Vrije Universiteit Brussel), André Matagne (Université de Liège, Liège, Belgium), and Annemarie Honegger for helpful discussions.

REFERENCES

1. Hamers-Casterman, C., Atarhouch, T., Muyldermans, S., Robinson, G., Hamers, C., Songa, E. B., Bendahman, N., and Hamers, R. (1993) Naturally occurring antibodies devoid of light chains, *Nature 363*, 446−448.
2. Decannière, K., Desmyter, A., Lauwereys, M., Ghahroudi, M. A., Muyldermans, S., and Wyns, L. (1999) A single-domain antibody fragment in complex with RNase A: non-canonical loop structures and nanomolar affinity using two CDR loops, *Structure Folding Des. 7*, 361−370.
3. Decannière, K., Muyldermans, S., and Wyns, L. (2000) Canonical antigen-binding loop structures in immunoglobulins: more structures, more canonical classes? *J. Mol. Biol. 300*, 83−91.
4. Spinelli, S., Frenken, L., Bourgeois, D., de Ron, L., Bos, W., Verrips, T., Anguille, C., Cambillau, C., and Tegoni, M. (1996) The crystal structure of a llama heavy chain variable domain, *Nat. Struct. Biol. 3*, 752−757.
5. Honegger, A., and Plückthun, A. (2001) Yet another numbering scheme for immunoglobulin variable domains: An automatic modeling and analysis tool, *J. Mol. Biol. 309*, 657−670.
6. Muyldermans, S., Cambillau, C., and Wyns, L. (2001) Recognition of antigens by single-domain antibody fragments: the superfluous luxury of paired domains, *Trends Biochem. Sci. 26*, 230−235.
7. Harmsen, M. M., Ruuls, R. C., Nijman, I. J., Niewold, T. A., Frenken, L. G., and de Geus, B. (2000) Llama heavy-chain V regions consist of at least four distinct subfamilies revealing novel sequence features, *Mol. Immunol. 37*, 579−590.
8. Muyldermans, S., Atarhouch, T., Saldanha, J., Barbosa, J. A., and Hamers, R. (1994) Sequence and structure of VH domain from naturally occurring camel heavy chain immunoglobulins lacking light chains, *Protein Eng. 7*, 1129−1135.
9. Wu, T. T., Johnson, G., and Kabat, E. A. (1993) Length distribution of CDRH3 in antibodies, *Proteins 16*, 1−7.
10. Arbabi Ghahroudi, M., Desmyter, A., Wyns, L., Hamers, R., and Muyldermans, S. (1997) Selection and identification of single domain antibody fragments from camel heavy-chain antibodies, *FEBS Lett. 414*, 521−526.
11. van der Linden, R. H., de Geus, B., Frenken, G. J., Peters, H., and Verrips, C. T. (2000) Improved production and function of llama heavy chain antibody fragments by molecular evolution, *J. Biotechnol. 80*, 261−270.
12. van der Linden, R. H., Frenken, L. G., de Geus, B., Harmsen, M. M., Ruuls, R. C., Stok, W., de Ron, L., Wilson, S., Davis, P., and Verrips, C. T. (1999) Comparison of physical chemical

properties of llama VHH antibody fragments and mouse monoclonal antibodies, *Biochim. Biophys. Acta 1431*, 37−46.
13. Desmyter, A., Transue, T. R., Ghahroudi, M. A., Thi, M. H., Poortmans, F., Hamers, R., Muyldermans, S., and Wyns, L. (1996) Crystal structure of a camel single-domain VH antibody fragment in complex with lysozyme, *Nat. Struct. Biol. 3*, 803−811.
14. Lauwereys, M., Arbabi Ghahroudi, M., Desmyter, A., Kinne, J., Holzer, W., De Genst, E., Wyns, L., and Muyldermans, S. (1998) Potent enzyme inhibitors derived from dromedary heavy-chain antibodies, *EMBO J. 17*, 3512−3520.
15. Knappik, A., Ge, L., Honegger, A., Pack, P., Fischer, M., Wellnhofer, G., Hoess, A., Wölle, J., Plückthun, A., and Virnekäs, B. (2000) Fully synthetic human combinatorial antibody libraries (HuCAL) based on modular consensus frameworks and CDRs randomized with trinucleotides, *J. Mol. Biol. 296*, 57−86.
16. Carter, P., Presta, L., Gorman, C. M., Ridgway, J. B., Henner, D., Wong, W. L., Rowland, A. M., Kotts, C., Carver, M. E., and Shepard, H. M. (1992) Humanization of an anti-p185HER2 antibody for human cancer therapy, *Proc. Natl. Acad. Sci. U.S.A. 89*, 4285−4289.
17. Krebber, A., Bornhauser, S., Burmester, J., Honegger, A., Willuda, J., Bosshard, H. R., and Plückthun, A. (1997) Reliable cloning of functional antibody variable domains from hybridomas and spleen cell repertoires employing a reengineered phage display system, *J. Immunol. Methods 201*, 35−55.
18. Bothmann, H., and Plückthun, A. (1998) Selection for a periplasmic factor improving phage display and functional periplasmic expression, *Nat. Biotechnol. 16*, 376−380.
19. Myers, J. K., Pace, C. N., and Scholtz, J. M. (1995) Denaturant *m* values and heat capacity changes: relation to changes in accessible surface areas of protein unfolding, *Protein Sci. 4*, 2138−2148.
20. Daniel, R. M., Dines, M., and Petach, H. H. (1996) The denaturation and degradation of stable enzymes at high temperatures, *Biochem. J. 317*, 1−11.
21. Saul, F. A., and Poljak, R. J. (1993) Structural patterns at residue positions 9, 18, 67 and 82 in the VH framework regions of human and murine immunoglobulins, *J. Mol. Biol. 230*, 15−20.
22. Faber, C., Shan, L., Fan, Z., Guddat, L. W., Furebring, C., Ohlin, M., Borrebaeck, C. A., and Edmundson, A. B. (1998) Three-dimensional structure of a human Fab with high affinity for tetanus toxoid, *Immunotechnology 3*, 253−270.
23. Graille, M., Stura, E., Corper, A., Sutton, B., Taussig, M., Charbonnier, J., and Silverman, G. (2000) Crystal structure of a *Staphylococcus aureus* protein A domain complexed with the Fab fragment of a human IgM antibody: structural basis for recognition of B-cell receptors and superantigen activity, *Proc. Natl. Acad. Sci. U.S.A. 97*, 5399−5404.
24. Fan, Z. C., Shan, L., Guddat, L. W., He, X. M., Gray, W. R., Raison, R. L., and Edmundson, A. B. (1992) Three-dimensional structure of an Fv from a human IgM immunoglobulin, *J. Mol. Biol. 228*, 188−207.
25. Marquart, M., Deisenhofer, J., Huber, R., and Palm, W. (1980) Crystallographic refinement and atomic models of the intact immunoglobulin molecule Kol and its antigen-binding fragment at 3.0 and 1.9 Å resolution, *J. Mol. Biol. 141*, 369−391.
26. Koradi, R., Billeter, M., and Wüthrich, K. (1996) MOLMOL: a program for display and analysis of macromolecular structures, *J. Mol. Graphics 14*, 29−32, 51−55.
27. Chien, N. C., Roberts, V. A., Giusti, A. M., Scharff, M. D., and Getzoff, E. D. (1989) Significant structural and functional change of an antigen-binding site by a distant amino acid substitution: proposal of a structural mechanism, *Proc. Natl. Acad. Sci. U.S.A. 86*, 5532−5536.
28. Novotny, J., Bruccoleri, R. E., and Haber, E. (1990) Computer analysis of mutations that affect antibody specificity, *Proteins 7*, 93−98.
29. Davies, J., and Riechmann, L. (1996) Single antibody domains as small recognition units: design and in vitro antigen selection of camelized, human VH domains with improved protein stability, *Protein Eng. 9*, 531−537.
30. Spinelli, S., Frenken, L. G., Hermans, P., Verrips, T., Brown, K., Tegoni, M., and Cambillau, C. (2000) Camelid heavy-chain variable domains provide efficient combining sites to haptens, *Biochemistry 39*, 1217−1222.
31. Jäger, M., Gehrig, P., and Plückthun, A. (2001) The scFv fragment of the antibody hu4D5-8: evidence for early premature domain interaction in refolding, *J. Mol. Biol. 305*, 1111−1129.
32. Jäger, M., and Plückthun, A. (1999) Folding and assembly of an antibody Fv fragment, a heterodimer stabilized by antigen, *J. Mol. Biol. 285*, 2005−2019.
33. Wörn, A., and Plückthun, A. (1999) Different equilibrium stability behavior of ScFv fragments: identification, classification, and improvement by protein engineering, *Biochemistry 38*, 8739−8750.
34. Perez, J. M., Renisio, J. G., Prompers, J. J., van Platerink, C. J., Cambillau, C., Darbon, H., and Frenken, L. G. (2001) Thermal unfolding of a llama antibody fragment: a two-state reversible process, *Biochemistry 40*, 74−83.
35. Davies, J., and Riechmann, L. (1994) "Camelising" human antibody fragments: NMR studies on VH domains, *FEBS Lett. 339*, 285−290.
36. Jäger, M., and Plückthun, A. (1999) Domain interactions in antibody Fv and scFv fragments: effects on unfolding kinetics and equilibria, *FEBS Lett. 462*, 307−312.
37. Wörn, A., and Plückthun, A. (2001) Stability engineering of antibody single-chain Fv fragments, *J. Mol. Biol. 305*, 989−1010.
38. Proba, K., Honegger, A., and Plückthun, A. (1997) A natural antibody missing a cysteine in VH: consequences for thermodynamic stability and folding, *J. Mol. Biol. 265*, 161−172.
39. Pace, C. N., and Scholtz, J. M. (1997) Measuring the conformational stability of a protein, in *Protein Structure, A Practical Approach* (Creighton, T. E., Ed.) pp 299−321, Oxford University Press, New York.
40. Kabat, E. A., Wu, T. T., Perry, H. M., Gottesmann, K. S., and Foeller, C. (1991) Variable region heavy chain sequences, in *Sequences of Proteins of Immunological Interest*, NIH Publication 91-3242, National Technical Information Service.

BI011239A